Electronic properties of oxygen-deficient and aluminum-doped rutile TiO_2 from first principles

Mazharul M. Islam,[1] Thomas Bredow,[2] and Andrea Gerson[1]
[1]*Applied Centre for Structural and Synchrotron Studies, University of South Australia, Mawson Lakes Campus, Mawson Lakes, Adelaide, South Australia 5095, Australia*
[2]*Institut für Physikalische und Theoretische Chemie, Universität Bonn, Wegelerstrasse 12, 53115 Bonn, Germany*
(Received 4 April 2007; published 20 July 2007)

The electronic properties of stoichiometric, defective, and aluminum-doped rutile TiO_2 have been investigated theoretically with periodic quantum-chemical calculations. Theoretical results obtained with the Perdew-Wang density functional method [Phys. Rev. B **45**, 13244 (1992)] and with a density functional-Hartree-Fock hybrid method are compared. Occupied defect states are observed in the band gap of rutile due to the presence of oxygen vacancies, which is in accord with previous theoretical studies and the experimentally observed coloring. For the investigation of aluminum doping, three different situations have been considered: substitution of a single Ti atom by an Al atom, cosubstitution of Ti by Al and O by Cl, and substitution of two Ti by two Al combined with the formation of an O vacancy. In the last two cases, aluminum doping does not introduce band gap states, and the band gap is even increased compared to undoped rutile. We conclude that stoichiometric Al doping reduces pigment coloring induced by oxygen vacancies in rutile and also suppresses the photocatalytic activity of titania pigments.

DOI: 10.1103/PhysRevB.76.045217 PACS number(s): 61.72.Ww, 71.15.Mb, 81.05.Je

I. INTRODUCTION

Titanium dioxide, TiO_2, has been studied extensively both experimentally and theoretically due to its particular physical and chemical properties: high refractive index, excellent optical transmittance in the visible and near-infrared regions, high dielectric constant,[1] and UV induced electron excitation.[2] It is used in heterogeneous catalysis, as a photocatalyst,[2] in solar cells for the production of hydrogen and electric energy, as a gas sensor, as white pigment, as colored ceramic pigment, as a corrosion-protective coating, as an optical coating, and in electronic and electrical devices.[3] It is also used in bone implants due to its high biocompatibility.[4] In surface science, titanium dioxide is considered as a model system for many metal oxides. Understanding its properties at fundamental level will help improve materials and device performance in many fields.

Titanium dioxide crystallizes in three different modifications: rutile, anatase, and brookite. Rutile is thermodynamically the most stable form. It has been chosen as the subject of this study. The rutile structure has a tetragonal unit cell (space group $D_{4h}^{14}-P4_2/mnm$) containing two titanium and four oxygen atoms. The lattice consists of hexagonal close packed oxygen atoms, with half of the octahedral spaces filled with titanium atoms (Fig. 1). One additional parameter u, the oxygen fractional coordinate, is necessary to define the crystal structure.

The electronic and optical properties of TiO_2 have been investigated experimentally using a wide range of methods: x-ray photoelectron spectroscopy,[5–8] x-ray absorption spectroscopy,[9–11] x-ray emission spectroscopy,[12] total electron yield (TEY) spectroscopy,[13] electron-energy-loss spectroscopy,[6,14–16] ultraviolet photoelectron spectroscopy (UPS),[17] resonant ultraviolet photoelectron spectroscopy,[18] absorption and photoluminescence spectroscopy,[19] and wavelength modulated transmission spectroscopy.[20] During the last years, accurate *ab initio* and density functional theory (DFT) electronic structure calculations have become available for the interpretation of TiO_2 spectroscopic data.

Theoretical investigations have been performed using the pseudopotential plane wave formalism both for DFT-local density approximation (LDA)[5,14,21–26] and Hartree-Fock (HF)[27] approaches. Self-consistent calculations using the linear muffin-tin orbital (LMTO) method,[12,13,28–30] tight binding model,[31–33] and extended Hückel molecular-orbital method[16] have also been performed to predict the electronic structure of TiO_2.

Defects, which may alter the electronic and optical properties of rutile, play an important role in technological applications of TiO_2. Naturally occurring rutile is almost always slightly reduced, leading to a pronounced color change of the crystal, from transparent to light and dark blue, which is accompanied by increased electrical conductivity.[34] The defect structure is assumed to be quite complex with combinations of various types of oxygen vacancies and Ti^{3+} and Ti^{4+} interstitials.[35] However, a recent theoretical investigation[26] has shown that the formation of oxygen vacancies is energetically more favorable than the insertion of titanium at interstitial sites. The defect structure varies with the oxygen vacancy concentration, which depends on temperature, gas pressure, metal impurities, etc.[36] At 1100 °C, an oxygen de-

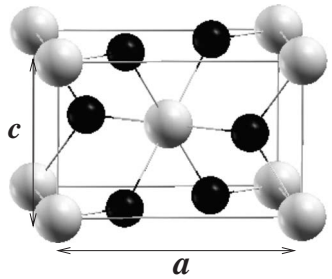

FIG. 1. Unit cell of rutile. Black spheres represent the oxygen atoms and light gray spheres represent the titanium atoms.

fect concentration of 0.5% under atmospheric pressure was measured.[36,37] Several experimental[3,17,34,38–41] and theoretical[26,35,42–48] investigations have been performed to understand the role of oxygen vacancies in TiO_2. These results will serve as a basis for comparison with the results presented here.

Titanium dioxide is well known as a photocatalyst. Its catalytic activity reduces the long-term durability of titania pigment materials. Upon UV irradiation, electrons (e^-) and holes (h^+) are created in the conduction band and valence band, respectively.[49] This process formally reduces titanium ions from Ti^{4+} to Ti^{3+}, causing coloration of the pigment. Commercial TiO_2 rutile pigments are always doped with Al_2O_3 to enhance photochemical stability. It is assumed that Al doping creates defects in the rutile lattice that act as traps for the photogenerated charges.[49,50] The presence of aluminum is also responsible for reducing particle agglomeration[51] and increasing the rate of anatase-to-rutile conversion during the chloride process.[51–54] In the present theoretical study, we investigate the possible sites of aluminum doping and the electronic properties of Al-doped rutile.

II. COMPUTATIONAL METHODS

The electronic and optical properties of TiO_2 for stoichiometric, oxygen-deficient, and Al-doped systems were calculated with periodic supercell models. In order to investigate the method dependence of the computed properties, two different quantum-chemical approaches were used, the Perdew-Wang exchange-correlation functional PWGGA[55,56] and the PW1PW DFT-HF hybrid method.[57] These methods have been applied for calculations of bulk properties of MgO, NiO, CoO,[57] $Li_2B_4O_7$,[58] B_2O_3,[59] and LiO_2,[60] defect properties of $Li_2B_4O_7$,[61] and electronic properties of Li_2O-B_2O_3 compounds.[62] In those studies, good agreement between calculated and experimental bulk properties was observed, in particular, for the PW1PW hybrid method.

The two methods were used as implemented in the crystalline orbital program CRYSTAL03.[63] In CRYSTAL, the Bloch functions are linear combinations of atomic orbitals. The quality of the atomic basis sets determines the reliability of the results. Therefore, we have used high quality atomic basis sets obtained from the literature. For titanium an 86-411(d31)G basis and for oxygen an 8-411G* basis were used, which have been successfully applied for the investigation of the electronic properties of rutile TiO_2 ultrathin films.[64] An 88-31G* basis was used for aluminum, which has been optimized for alumina.[65] For chlorine, an 86-311G basis was used, which has been optimized for the structural properties investigation of NaCl.[66]

A primitive unit cell containing two formula units was used as model for stoichiometric rutile. The projected density of states (PDOS) was calculated using the Fourier-Legendre technique[67] with a *Monkhorst net*[68] using shrinking factors $s=8$. In order to minimize direct defect-defect interaction between neighboring cells, we used supercells ($Ti_{16}O_{32}$, $Ti_{32}O_{64}$, and $Ti_{54}O_{108}$) as models of the defective bulk.

III. RESULTS AND DISCUSSION

A. Bulk properties of rutile

The optimized structure parameters a, c, and u, the cohesive energy per TiO_2 unit E_u, the band gap E_g, and the bulk modulus B_0 obtained with PW1PW and PWGGA are given in Table I together with the corresponding experimental values. The lattice parameters correspond to an extrapolation of experimental x-ray data to $T=0$ K.[69,70] The calculated lattice parameters obtained with the two methods are close to the experimental values. The largest deviation, +0.9%, is obtained for the PWGGA value of a. This is better than the error of −2% obtained by previous DFT-LDA calculations.[71] However, the structural parameters obtained with PWGGA are in good agreement with a previous CRYSTAL-PWGGA study by Muscat *et al.*[72] The hybrid method PW1PW gives a slightly better reproduction of experimental structure properties than PWGGA.

TABLE I. Comparison of calculated structural parameters a (Å), c (Å), and u, binding energy E_u (in parentheses are the temperature corrected values) (kJ/mol), bulk modulus B_0 (GPa), and band gap E_g (eV) with experiment.

	PWGGA	PW1PW	Expt.
a	4.63	4.59	4.59[a]
c	2.98	2.98	2.96[a]
u	0.305	0.305	0.305[a]
E_u	−2054 (−2036)	−1929 (−1909)	−1915[a]
B_0	223	234	216[b]
E_g	1.90	3.54	3.03[c]

[a]Reference 70.
[b]Reference 74.
[c]Reference 19.

The experimental value of E_u for rutile is 1915 kJ/mol.[70] Theoretical estimates of E_u are obtained by subtracting the total energies of the free atoms in their ground states with converged basis sets from the energy of the periodic system. In this way, temperature effects and contributions from zero point energy are neglected. They have been taken into account *a posteriori* by a frequency calculation with CRYSTAL06.[73] The sum of all correction terms is +18 kJ/mol for PWGGA and +20 kJ/mol for PW1PW. The corrected value of E_u is −1909 kJ/mol at the PW1PW level, which is in excellent agreement with the experimental reference (−1915 kJ/mol). The PWGGA method overestimates E_u considerably (−2036 kJ/mol).

The experimental value of 216 GPa for the bulk modulus (B_0) has been determined under ambient conditions.[74] A recent x-ray spectroscopy study[75] has obtained a value of 230±20 GPa. We find isothermal bulk moduli of 234 and 223 GPa with PW1PW and PWGGA, respectively, which are in excellent agreement with the experimental range.

Rutile is a semiconductor with a band gap (E_g) of 3.03 eV.[19] In the present study, the band structure was computed along the direction that contains the highest number of high-symmetry points within the Brillouin zone,[76] namely, $Z \rightarrow A \rightarrow M \rightarrow \Gamma \rightarrow Z \rightarrow R \rightarrow X \rightarrow \Gamma$. The band structure obtained with PW1PW is shown in Fig. 2. The calculated E_g values obtained with PW1PW and PWGGA are given in Table I, and the minimal vertical transition (MVT) and minimal indirect transition (MIT) energies are given in Table II.

Both methods predict a *direct* gap at Γ. Experimental in-

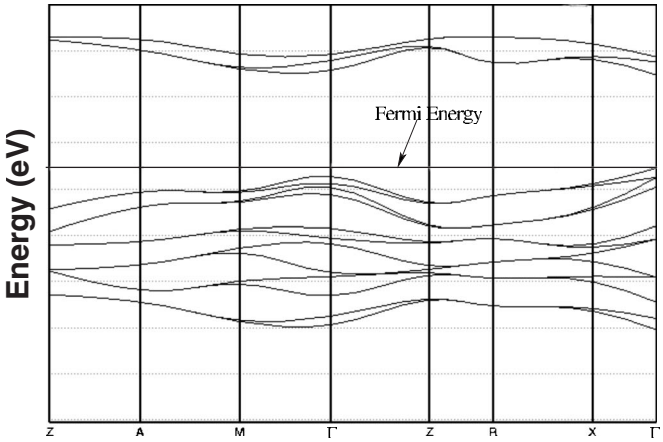

FIG. 2. Band structure of rutile TiO_2 (PW1PW results).

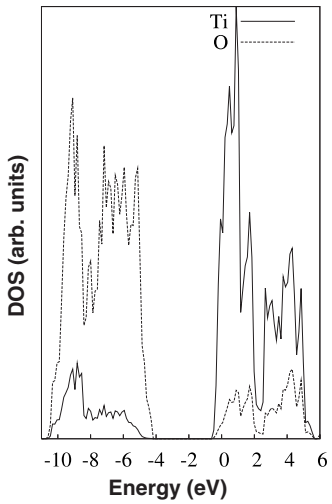

FIG. 3. Density of states of rutile TiO_2 (PW1PW results).

vestigations using absorption and photoluminescence spectroscopy,[19] and wavelength modulated transmission spectroscopy[20] have also determined that rutile is a direct-forbidden-gap semiconductor, i.e., the direct transition is dipole forbidden. The MVT is along the Γ-Γ direction. The MVT value obtained with PW1PW is 3.54 eV, slightly overestimating the experimental value of 3.03 eV.[19,20] The pure DFT-PWGGA approach (1.90 eV) underestimates the direct transition energy by 1.13 eV. This is similar to the DFT-LDA-based direct forbidden gaps of 2.0 eV,[22] 1.87 eV,[25] and 1.7 eV.[26] The gradient corrections therefore do not considerably improve the LDA band gap, while the inclusion of exact Hartree-Fock exchange leads to an overestimation of E_g.

In agreement with previous theoretical investigations,[22,27] our calculations also predict that rutile has the smallest indirect gap along the Γ-*M* direction. The MIT energies, 3.82 and 2.04 eV with PW1PW and PWGGA, respectively, are close to the corresponding MVT energies. However, according to Mathieu *et al.*,[20] the indirect gap shows a nonlinear behavior under [100] compression, which should include the transition along the *X* direction. It is therefore possible that the indirect transition along the Γ-*X* direction, the second MIT, has the highest probability although its calculated transition energy is slightly greater than that for the Γ-*M* direction (Table II).

The DOS calculated with PW1PW is shown in Fig. 3. The calculated valence band width is about 6.3 eV, in good agreement with the range of experimental values, 5–6 eV.[5–8,12] The valence band (VB) is mainly composed of O 2*p* states with some hybridization with Ti 3*d* orbitals.

The PDOS of Ti obtained with x-ray photoelectron spectroscopy[5] shows a splitting of two major peaks by 2.3 eV. In our case, the center-to-center separation of the Ti peaks is 2.2 eV. This is in good agreement with the experimental result. According to ligand-field theory,[77] the presence of two Ti peaks in the VB is a result of the splitting of Ti 3*d* orbitals into states with t_{2g} and e_g symmetries. t_{2g} states have a lower energy than e_g states. These states are mirrored in the structure of the PDOS for O. A similar picture was observed in previous combined theoretical and experimental studies,[5,12] and a theoretical DFT-LDA study.[22] The t_{2g} and e_g states represent the π and σ Ti *d* orbitals hybridized with O 2*p* states.

Similar to the VB, the conduction band (CB) is also composed of both Ti 3*d* and O 2*p* states. The bottom of the conduction band is mainly formed by Ti 3*d* states, their contribution being several times higher than that of O 2*p* states. This is in good agreement with the experimental finding from TEY spectroscopy.[13]

TABLE II. Minimum vertical electronic transition (MVT) and minimum indirect transition (MIT) energies (eV).

			MVT				
	Z-Z	*A-A*	*M-M*	Γ-Γ	*Z-Z*	*R-R*	*X-X*
PW1PW	6.68	5.50	4.92	3.54	6.68	4.96	5.33
PWGGA	4.60	3.60	3.12	1.90	4.60	3.13	3.39
			MIT				
	A-M	*M*-Γ	Γ-*M*	Γ-*Z*	*Z-R*	*X*-Γ	Γ-*X*
PW1PW	4.56	4.77	3.82	5.07	5.53	4.43	4.58
PWGGA	2.74	2.96	2.04	3.14	3.62	2.57	2.69

TABLE III. Formation energy of neutral oxygen vacancies $E_{de}(V)$ (kJ/mol) as function of the defect concentration c (%) (unrel=unrelaxed, rel=relaxed).

		$E_{de}(V)$						
		PWGGA				PW1PW		
Supercell	c	Unrel	Rel	Unrel[a]	Rel[a]	Unrel	Rel	Expt.[b]
Ti_2O_4	25.0	630	614	679	651	653	642	
$Ti_{16}O_{32}$	3.1	595	510	637	568	635	583	
$Ti_{32}O_{64}$	1.6	542	445			575	514	
$Ti_{54}O_{108}$	0.9	519	431			530	490	
								439

[a]Closed-shell singlet state calculations.
[b]Reference 36.

B. Oxygen vacancies in rutile

The experimentally measured oxygen vacancy concentration in rutile is 0.5% at 1100 °C and near atmospheric pressure.[36,37] The enthalpy of formation of oxygen vacancies has been measured as 439 kJ/mol.[36] An infrared absorption study[34] measured that neutral O defects produce a peak 1.18 eV below the bottom of the bulk CB. In a UPS study of the surface electronic structure, Henrich and Kurtz[40] identified an occupied defect state 1.2 eV below the CB due to the presence of oxygen vacancies. A 1.61 eV peak below the conduction band has been found in a UV spectrum[41] and attributed to a positively charged O defect.

Chen *et al.*[42] investigated oxygen-deficient rutile theoretically. They employed an embedded-cluster numerical discrete variation method. A defect peak was observed 0.87 eV below CB for neutral defects, and 1.78 eV below CB for positively charged defects. A similar result was obtained in a recent LMTO study of the neutral O defect in rutile.[47] An occupied defect state was found 0.8 eV below the CB bottom edge. The two extra electrons left behind by the oxygen were distributed on the three Ti atoms surrounding the vacancy. Rutile with charged O defects is reported to have partially occupied defect band states, but their positions relative to the CB bottom are not given. However, the latter investigation can be regarded as incomplete, since lattice relaxation was neglected. Another theoretical investigation[35] based on a semiempirical self-consistent method found the oxygen vacancy peak 0.7 eV below CB. At DFT-LDA[26,44] and DFT-PWGGA[45] levels, the gap states are located 0.1 and 0.3 eV below CB, respectively. These differences are considerably smaller than the experimental values.[34,38,40]

In the present study, a systematic investigation is performed for the oxygen vacancy formation energy, $E_{de}(V)$, the effect of relaxation, and the optical transition energies of defective rutile. Supercells ($Ti_{16}O_{32}$, $Ti_{32}O_{64}$, and $Ti_{54}O_{108}$) were used for the defect calculations. The lowest vacancy concentration that we studied here is therefore 0.9%, which is still larger than the experimentally measured value (0.5%). For lower defect concentrations, one has to consider larger supercells. This was not possible due to limited computer resources.

1. Defect formation and structural relaxation

The defect formation energy of a neutral oxygen vacancy $E_{de}(V)$ is calculated as

$$E_{de}(V) = E(\mathrm{Ti}_n\mathrm{O}_{2n-1}) + 1/2E(\mathrm{O}_2) - E(\mathrm{Ti}_n\mathrm{O}_{2n}). \quad (3.1)$$

Here, $E(\mathrm{Ti}_n\mathrm{O}_{2n-1})$ and $E(\mathrm{Ti}_n\mathrm{O}_{2n})$ denote the total energies of the supercell with and without defect, respectively. $E(\mathrm{O}_2)$ is the ground-state energy of the oxygen molecule after optimization. Charged oxygen defects could not be studied with CRYSTAL because the energy and energy gradient expressions are not correctly implemented for charged cells with a compensating homogeneous background charge.[73]

$E_{de}(V)$ obtained with PWGGA and PW1PW are presented in Table III for unrelaxed and fully relaxed systems. The basis functions of the oxygen ion were left at the defect position. Calculations for the triplet state were performed using the unrestricted Kohn-Sham (UKS) method. The removal of oxygen leaves two electrons in the VB that previously occupied O $2p$ levels. It is known[34,40,45–47] that these unpaired electrons are mainly localized in the $3d$ orbitals of the neighboring Ti atoms. Closed-shell singlet state calculations were also performed with the PWGGA method. It was found that $E_{de}(V)$ for the singlet state is 37–58 kJ/mol larger than the corresponding value of the triplet state. Therefore, closed-shell singlet state calculations are not considered further.

$E_{de}(V)$ decreases with decreasing defect concentration (i.e., increasing supercell size). This indicates a long-range repulsive interaction between oxygen vacancies located in neighboring cells. The observed trend can also be due to the effect of relaxation of the lattice atoms around the vacancy, most probably of electrostatic origin. The movement of the atoms out of their lattice positions due to the presence of the defect is restricted by the periodic boundary conditions introduced on the supercell. This can be best seen by the very small relaxation energy (difference between unrelaxed and fully relaxed defect formation energies) of the smallest supercell (Ti_2O_4), 11 kJ/mol (PW1PW) and 16 kJ/mol (PWGGA). For the larger supercells ($Ti_{16}O_{32}$, $Ti_{32}O_{64}$, and $Ti_{54}O_{108}$), the relaxation energy is considerably larger, 85–97 kJ/mol with PWGGA and 52–61 kJ/mol with

TABLE IV. Distances r (Å) of neighboring atoms from the vacancy site and changes of the distances Δr (%) for the relaxed atoms in $Ti_{32}O_{64}$ obtained with PW1PW.

Atom	r	Unrelaxed	Relaxed	Δr (%)
Ti(2)	r_1	1.95	2.11	+8.2
Ti(1)	r_2	1.98	2.12	+7.1
O(1)	r_3	2.53	2.52	−0.4
O(8)	r_4	2.78	2.74	−1.4
O(2)	r_5	2.98	2.98	0.0
O(2)	r_6	3.32	3.32	0.0

PW1PW. This indicates that relaxation is important for the study of defective systems. The PWGGA method generally gives smaller values of $E_{de}(V)$ than PW1PW, which can be partly traced back to the larger relaxation energy. For the smallest defect concentration (0.9%), $E_{de}(V)$ is 431 kJ/mol with PWGGA and 490 kJ/mol with PW1PW. This trend is in line with our previous observation for the defect formation energies in Li_2O (Ref. 60) and $Li_2B_4O_7$ (Ref. 61). The PWGGA defect formation energy agrees well with the calculated value of 4.44 eV (428 kJ/mol) obtained by Cho *et al.* at the local spin density approximation level.[26] Both DFT values are in better agreement with the experimental value [439 kJ/mol (Ref. 36)] than the PW1PW method, in contrast to our previous experience for other oxides. However, the convergence of $E_{de}(V)$ with respect to the supercell size is slow. It is therefore possible that the defect formation energy for larger supercells, which better represent the experimentally observed defect concentration (0.5%), is smaller than those reported here. In such case, the PWGGA method would underestimate the experimental defect formation energy value, whereas the PW1PW approach would be in better agreement with the experimental value.

The structural relaxation effects for the O vacancy are investigated by measuring the changes of distances of the relaxed atoms from the vacancy site. PW1PW results for the relaxation effects are shown in Table IV. The PWGGA method gives the same trend. Prior to relaxation, the vacancy site is surrounded by two nearest-neighbor (1-NN) Ti atoms at a distance of 1.95 Å and by one Ti atom at a distance of 1.98 Å (2-NN). Ti 1-NN and 2-NN atoms move away from the vacancy, by 8.2% and 7.1%, respectively. This is reasonable since the Ti ions are positively charged and should, therefore, repel each other as the central oxygen is removed. The trend is in agreement with DFT-LDA investigations performed by Cho *et al.*[26] and Ramamoorthy *et al.*,[44] where a relaxation of +0.27–0.30 and +0.1 Å, respectively, was observed.

The 3-NN and 4-NN O atoms show a small inward relaxation of 0.4% and 1.4%. The positions of 5-NN and 6-NN O atoms are virtually unchanged.

2. Optical transition energies of oxygen-deficient rutile

The experimental value of the optical transition energy for neutral oxygen-deficient rutile is 1.2 eV,[34,40] indicating a doubly occupied defect level below the bottom of the conduction band edge. A charged O defect introduces a partially filled defect level at about 1.61 eV below the conduction band.[41] The DOS curves for defective $Ti_{16}O_{31}$ supercell using PW1PW are shown in Fig. 4.

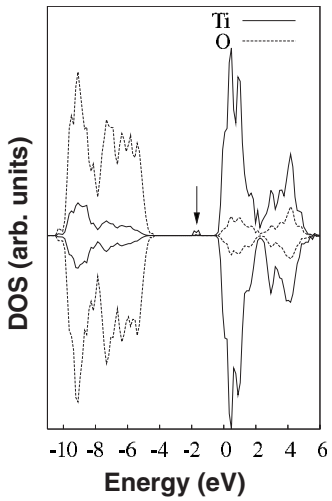

FIG. 4. Total density of states for α and β electrons of rutile TiO_2 containing a neutral oxygen vacancy (PW1PW results).

We have tested different spin distributions over Ti atoms near the defect site for all the considered supercells. The most stable structures have been selected for further investigation. The two electrons which are trapped in the defective supercell are strongly localized in the 3*d* orbitals of the 1-NN and 2-NN Ti atoms. The spin density is highest at the two 1-NN Ti atoms (0.82 a.u.), and only 0.23 a.u. on the 2-NN Ti atom. The PWGGA method gives a similar spin density distribution as the PW1PW method, with a less pronounced localization on the two nearest Ti atoms. This is in accordance with the results of a recent DFT-LDA investigation.[26] Previous theoretical investigations on defective surfaces of rutile[42,46,48] also concluded that the electrons are localized on two fivefold-coordinated titanium atoms, rather than on the defect site. The same conclusion was also obtained experimentally.[3,39]

The calculated band gaps of the defective systems as function of the supercell size are presented in Table V. The band gap increases with increasing size of the supercell, i.e., with decreasing defect concentration. However, its value is nearly converged with the largest considered supercell. For the larger supercells, PW1PW (0.99–1.06 eV) gives the best

TABLE V. Calculated values of band gap E_g (eV) for the defective supercells.

	E_g		
Supercell	PWGGA	PW1PW	Expt.[a]
Ti_2O_4	0.13	0.51	
$Ti_{16}O_{32}$	0.25	1.06	1.18
$Ti_{32}O_{64}$	0.21	0.99	

[a]References 34 and 40.

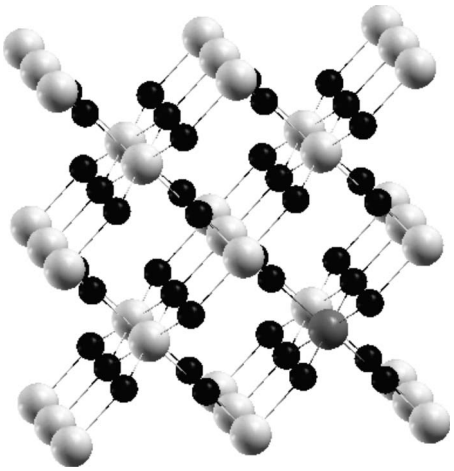

FIG. 5. Supercell $Ti_{15}AlO_{32}$, doublet state; black spheres represent the oxygen atoms, light gray spheres represent the titanium atoms, and dark gray sphere represents the aluminum atom.

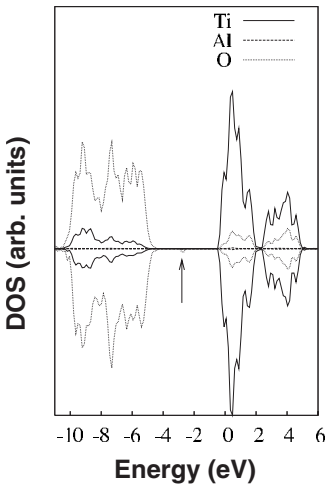

FIG. 6. Total density of states for α and β electrons of aluminum-doped TiO_2 in the substitutional site (PW1PW results).

reproduction of the experimental optical absorption energy [1.18 eV (Refs. 34 and 40)], whereas PWGGA gives much too small values, 0.21–0.25 eV. Our PWGGA result is in line with previous DFT-LDA studies which gave 0.2 eV (Ref. 26) and 0.3 eV (Ref. 44), and a PWGGA[45] value of 0.1 eV.

The underestimation of the optical transition by pure DFT methods can be related to the artificial self-interaction which is a consequence of the approximate nature of the exchange-correlation functionals. Moreover, care must be taken in general when comparing DFT one-particle energies with data from optical spectroscopy which correspond to energetic differences of many-electron states. Quantitative agreement should therefore not be expected. The hybrid method, on the other hand, was parametrized to reproduce optical transitions[57] and should therefore better agree with experiment.

C. Al^{3+}-doped TiO_2

There have been many investigations of the structure of aluminum dopants within the rutile crystal lattice. The results are controversial. It is found that Al^{3+} ions occupy Ti substitutional sites,[52,78–80] interstitial sites,[49,81–83] a combination of both sites,[83–85] or Ti substitutional sites in combination with oxygen vacancies.[49,82,83,86] A UV-visible spectroscopic study[49] found that the Al^{3+} substitutional doping in combination with oxygen vacancies seems to suppress TiO_2 photoactivity. On the other hand, the interstitially incorporated Al^{3+} has no effect on the photoactivity. In a recent semiempirical study, Steveson *et al.*[87] demonstrated that a single substitution of Ti by Al and two substitutions of Ti by Al combined with one oxygen vacancy are energetically favorable over interstitial Al doping. In the present study, substitutional Al^{3+} doping with and without an oxygen vacancy, and with cosubstitution of oxygen by chlorine is examined.

1. Substitutional Al doping

A $Ti_{16}O_{32}$ supercell was employed for the defect calculations. One Ti atom was substituted by an Al atom (Fig. 5). In this model, the lattice remains neutral but an unpaired electron is introduced. It is treated with the UKS method. It is observed that the unpaired electron introduced due to the formal substitution of Ti^{4+} by Al^{3+} is localized on one of the oxygen atoms nearest Al^{3+}. Thus, one oxygen which was formally O^{2-} becomes O^{-}. Initially, the Al is surrounded by four oxygen atoms at a distance of 1.95 Å. After optimization, the average Al-O distance decreases to 1.92 Å.

The electronic properties of the singly Al-doped rutile were investigated by calculating the total density of states (DOS). The DOS obtained with PW1PW is shown in Fig. 6. There is an unoccupied defect state 2.8 eV above the valence band maximum which is marked by an arrow. This minority spin state is composed of oxygen 2*p* orbitals. The band gap is reduced to 1.6 eV, which would make the oxide colored. This is in contradiction to the experimental observation that Al-doped rutile is colorless.[49] Therefore, we conclude that the nonstoichiometric substitution of Ti^{4+} by Al^{3+} in rutile is not likely.

2. Substitutional Al doping in combination with chloride counterion

The formal charge (−1) produced by the substitution of one Ti^{4+} by Al^{3+} can be compensated by a counterion (Cl^{-}) substituting an oxygen ion (formally O^{2-}). White titania pigments are commonly manufactured via the chloride process where titanium tetrachloride reacts with oxygen at temperatures between 1300 and 1700 K.[51] $AlCl_3$ is also added to increase the rate of anatase-to-rutile transformation.[51–54] Therefore, it is assumed that the chloride counterion is involved in the photostabilization of commercial rutile pigments. In our models, this is realized by replacing one oxygen by chlorine in addition to a substitution of Ti by Al. As the most likely substitution site, we chose the lattice oxygen that was reduced to O^{-} after substitution of Ti by Al as described in the previous section.

The distance between Al and Cl is 1.95 Å before relaxation. After optimization, the Al-Cl distance increases to 2.20 Å, corresponding to an outward relaxation of Cl by

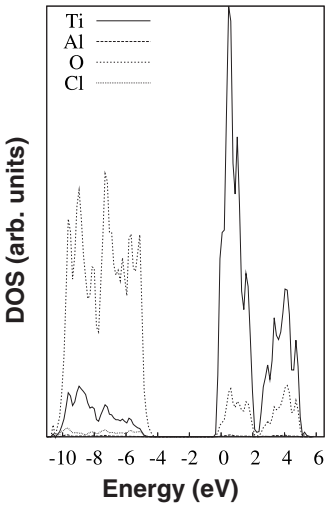

FIG. 7. Total density of states for the aluminum-doped TiO_2 in combination with chloride counterion (PW1PW results).

13% (PW1PW level). The PWGGA method gives a similar trend for the relaxation.

The DOS (Fig. 7) calculated with PW1PW for a $Ti_{15}AlClO_{31}$ supercell shows no gap state. As in the undoped system, the VB is mainly composed of oxygen states (with a smaller contribution from titanium states) and the CB is mainly composed of titanium states (with a smaller contribution from oxygen states). There are very small contributions from aluminum and chlorine states in the valence band. The Fermi energy is unchanged compared to the defect-free situation but the bottom of the conduction band is shifted to higher energy. Therefore, the band gap increased by 0.18 eV (PW1PW) and 0.09 eV (PWGGA), compared to undoped rutile (Table VI). These results indicate that combined substitution of Ti by Al and O by Cl can be responsible for the observed deactivation of rutile pigments.

3. Substitutional Al doping in combination with an oxygen vacancy

Two closest Ti atoms (distance=2.98 Å) were substituted by Al in a $Ti_{16}O_{32}$ supercell. The resulting formal charge (−2) was compensated by an oxygen vacancy (Fig. 8) at a site bridging the two Al atoms.

The distribution of two aluminum atoms and one oxygen vacancy in the supercell was varied and the relative stability of various local configurations was calculated. Instead of substituting only two nearest titanium atoms, two next-nearest titanium atoms (distance=3.57 Å) were also substituted by aluminum atoms. Another test calculation was performed by moving the oxygen vacancy at the next-nearest distance (1.98 Å instead of 1.95 Å). In both cases, the systems are less stable than the first considered case where the two Al atoms are nearest neighbors of the oxygen vacancy. After optimization, three out of four Al-O distances decreased from 1.95 to 1.85 Å. One Al-O distance increased to 2.20 Å, similar to the Al-Cl distance reported in the previous section.

TABLE VI. Comparison of calculated band gap energies E_g (eV) for doped and undoped rutile.

	E_g		
Method	$Ti_{15}AlClO_{31}$	$Ti_{14}Al_2O_{31}$	Undoped
PW1PW	3.72	3.65	3.54
PWGGA	1.99	1.95	1.90

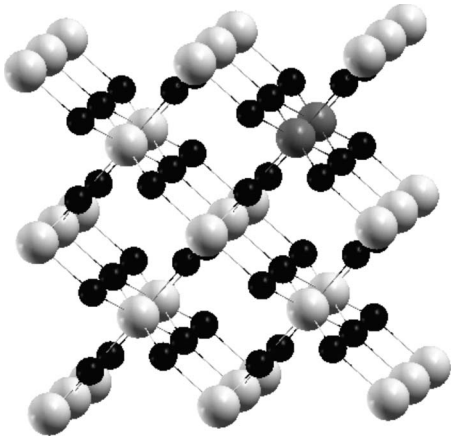

FIG. 8. Supercell $Ti_{14}Al_2O_{31}$; black spheres represent oxygen atoms, light gray spheres represent titanium atoms, and gray spheres represent aluminum atoms.

The DOS of the $Ti_{14}Al_2O_{31}$ supercell calculated with PW1PW is shown in Fig. 9. The Fermi energy is unchanged compared to the undoped system, while the bottom of the conduction band is slightly shifted to higher energies, thus increasing the band gap (Table VI).

The band gap of rutile decreased due to the presence of oxygen vacancies (Table V). The oxygen vacancy introduces occupied defect levels in the bulk band gap, leading to a pronounced color change of the crystal. In contrast, doping

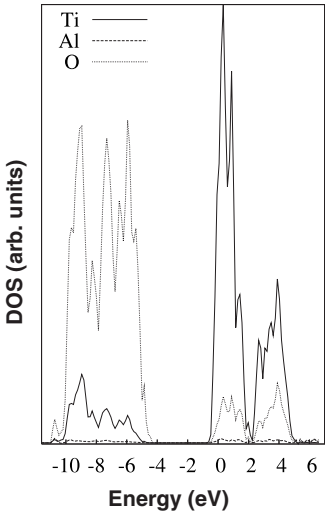

FIG. 9. Total density of states for Al-doped TiO_2 in combination with an oxygen vacancy (PW1PW results).

with Al in substitutional sites in combination with an oxygen vacancy does not introduce any defect level in the band gap, since the extra electrons induced by the oxygen vacancy are compensated by the Al ions. In this way, the rutile band gap has slightly increased compared to the undoped system. Therefore, aluminum doping does not introduce any color to the pigment nor does it change the electronic nature of rutile, which remains a semiconductor.[88] This is in good agreement with experiments.[49,89]

IV. SUMMARY AND CONCLUSION

The structural, energetic, and electronic properties of stoichiometric and defective TiO_2 were investigated by means of quantum-chemical calculations and compared to available experimental data. The comparison of the optimized lattice parameters with experiment shows that the considered methods give a good reproduction of experimental values. The hybrid method PW1PW gives reasonable agreement with experiment for the calculated energetic and electronic properties, while PWGGA overestimates the binding energy and underestimates the band gap. The calculated values of the oxygen vacancy formation energy for the largest supercell considered here ($Ti_{54}O_{108}$) are 431 (PWGGA) and 490 (PW1PW) kJ/mol, which are in the range of experimental enthalpy of oxygen vacancy formation. Relaxation around oxygen vacancies is found to be restricted to the nearest-neighbor Ti atoms. The removal of a neutral oxygen atom from the rutile lattice leads to the formation of occupied defect levels below the bottom of the conduction band edge. The extra electrons are mainly localized in 3*d* orbitals of the two Ti atoms nearest the vacancy. The band gap is reduced considerably compared to that of the nondefective bulk system. Local *d*-*d* transitions are possible and therefore the pigment will appear colored. The best agreement between the calculated excitation energy and optical spectroscopy was obtained with the PW1PW approach.

The substitution of a single Ti by Al introduces an unpaired electron which is localized on one of the oxygen atoms closest to Al. An unoccupied peak in the beta ladder appears, which reduces the band gap to 1.6 eV. This would make the system colored, which contradicts the general purpose of Al doping and disagrees with experimental observation. Therefore, we conclude that the nonstoichiometric substitution is not likely to occur in the chloride process. Charge compensation by additional substitution of O by Cl removes the defect level. In that case, the band gap is even slightly increased compared to that in the undoped system. A similar electronic structure is obtained by substitution of two Ti^{4+} by Al^{3+} together with the formation of an oxygen vacancy. Therefore, stoichiometric rutile doping with Al is predicted to enhance the photostability of the pigment as compared to O deficient pigments.

ACKNOWLEDGMENTS

We would like to acknowledge the funding provided by the Australian Research Council (ARC) Linkage grant "Electronic and Optical Properties of Doped Titanium Dioxide" and provision of Visiting Researcher funding by the University of South Australia.

[1] H.-S. Kim, D. C. Gilmer, S. A. Campbell, and D. L. Polla, Appl. Phys. Lett. **69**, 3860 (1996).
[2] A. Fujishima and K. Honda, Nature (London) **238**, 37 (1972).
[3] U. Diebold, Surf. Sci. Rep. **48**, 53 (2003).
[4] F. H. Jones, Surf. Sci. Rep. **42**, 75 (2001).
[5] J. C. Woicik, E. J. Nelson, L. Kronik, M. Jain, J. R. Chelikowsky, D. Heskett, L. E. Berman, and G. S. Herman, Phys. Rev. Lett. **89**, 077401 (2002).
[6] W. Göpel, J. A. Anderson, D. Frankel, M. Jaehnig, K. Phillips, J. A. Schäfer, and G. Rocker, Surf. Sci. **139**, 333 (1984).
[7] S. Hüfner and G. K. Wertheim, Phys. Rev. B **8**, 4857 (1973).
[8] P. Kowalczyk, F. R. McFeely, L. Ley, V. T. Gritsyna, and D. A. Shirley, Solid State Commun. **23**, 161 (1977).
[9] F. M. F. de Groot, M. Grioni, J. C. Fuggle, J. Ghijsen, G. A. Sawatzky, and H. Petersen, Phys. Rev. B **40**, 5715 (1989).
[10] G. van der Laan, Phys. Rev. B **41**, 12366 (1990).
[11] L. A. Grunes, Phys. Rev. B **27**, 2111 (1983).
[12] L. D. Finkelstein, E. Z. Kurmaev, M. A. Korotin, A. Moewes, B. Schneider, S. M. Butorin, J.-H. Guo, J. Nordgren, D. Hartmann, M. Neumann, and D. L. Ederer, Phys. Rev. B **60**, 2212 (1999).
[13] L. D. Finkelstein, E. I. Zabolotzky, M. A. Korotin, S. N. Shamin, S. M. Butorin, E. Z. Kurmaev, and J. Nordgren, X-Ray Spectrom. **31**, 414 (2002).
[14] N. Vast, L. Reining, V. Olevano, P. Schattschneider, and B. Jouffrey, Phys. Rev. Lett. **88**, 037601 (2002).
[15] M. H. Mohamed, H. R. Sadeghi, and V. E. Henrich, Phys. Rev. B **37**, 8417 (1988).
[16] L. A. Grunes, R. D. Leapman, C. N. Wilker, R. Hoffmann, and A. B. Kunz, Phys. Rev. B **25**, 7157 (1982).
[17] R. H. Tait and R. V. Kasowski, Phys. Rev. B **20**, 5178 (1979).
[18] Z. Zhang, S.-P. Jeng, and V. E. Henrich, Phys. Rev. B **43**, 12004 (1991).
[19] A. Amtout and R. Leonelli, Phys. Rev. B **51**, 6842 (1995).
[20] H. Mathieu, J. Pascual, and J. Camassel, Phys. Rev. B **18**, 6920 (1978).
[21] S. B. Sinnott, R. F. Wood, and S. J. Pennycook, Phys. Rev. B **61**, 15645 (2000).
[22] K. M. Glassford and J. R. Chelikowsky, Phys. Rev. B **46**, 1284 (1992).
[23] K. M. Glassford, N. Troullier, J. L. Martins, and J. R. Chelikowsky, Solid State Commun. **76**, 635 (1990).
[24] D. C. Allan and M. P. Teter, J. Am. Ceram. Soc. **73**, 3247 (1990).
[25] C. Lee, P. Ghosez, and X. Gonze, Phys. Rev. B **50**, 13379 (1994).
[26] E. Cho, S. Han, H.-S. Ahn, K.-R. Lee, S. K. Kim, and C. S. Hwang, Phys. Rev. B **73**, 193202 (2006).
[27] B. Silvi, N. Fourati, R. Nada, and C. R. A. Catlow, J. Phys. Chem. Solids **52**, 1005 (1991).
[28] N. I. Medvedeva, V. P. Zhukov, M. Ya. Khodos, and V. A. Gubanov, Phys. Status Solidi B **160**, 517 (1990).
[29] M. A. Khan, A. Kotani, and J. C. Parlebas, J. Phys.: Condens.

Matter **3**, 1763 (1991).
[30] B. Poumellec, P. J. Durham, and G. Y. Guo, J. Phys.: Condens. Matter **3**, 8195 (1991).
[31] P. K. Schelling, N. Yu, and J. W. Halley, Phys. Rev. B **58**, 1279 (1998).
[32] S. Munnix and M. Schmeits, Phys. Rev. B **30**, 2202 (1984).
[33] N. Daude, C. Gout, and C. Jouanin, Phys. Rev. B **15**, 3229 (1977).
[34] D. C. Cronemeyer, Phys. Rev. **113**, 1222 (1959).
[35] N. Yu and J. W. Halley, Phys. Rev. B **51**, 4768 (1995).
[36] P. Kofstad, *Nonstoichiometry, Diffusion, and Electrical Conductivity in Binary Metal Oxides* (Wiley, New York, 1972), Chap. 8.
[37] T. Bak, J. Nowotny, and M. K. Nowotny, J. Phys. Chem. B **110**, 21560 (2006).
[38] V. E. Henrich, G. Dresselhaus, and H. J. Zeiger, Phys. Rev. Lett. **36**, 1335 (1976).
[39] M. A. Henderson, Surf. Sci. **400**, 203 (1998).
[40] V. E. Henrich and R. L. Kurtz, Phys. Rev. B **23**, 6280 (1981).
[41] T.-C. Lu, Ph.D. thesis, SiChuan University, 1997.
[42] J. Chen, L.-B. Lin, and F.-Q. Jing, J. Phys. Chem. Solids **62**, 1257 (2001).
[43] S. Munnix and M. Schmeits, Phys. Rev. B **31**, 3369 (1985).
[44] M. Ramamoorthy, R. D. King-Smith, and D. Vanderbilt, Phys. Rev. B **49**, 7709 (1994).
[45] P. J. D. Lindan, N. M. Harrison, M. J. Gillan, and J. A. White, Phys. Rev. B **55**, 15919 (1997).
[46] T. Bredow and G. Pacchioni, Chem. Phys. Lett. **355**, 417 (2002).
[47] V. I. Anisimov, M. A. Korotin, I. A. Nekrasov, A. S. Mylnikova, A. V. Lukoyanov, J. L. Wang, and Z. Zeng, J. Phys.: Condens. Matter **18**, 1695 (2006).
[48] W. C. Mackrodt, E.-A. Simson, and N. M. Harrison, Surf. Sci. **384**, 192 (1997).
[49] U. Gesenhues, J. Photochem. Photobiol., A **139**, 243 (2001).
[50] Z. Luo and Q. Gao, J. Photochem. Photobiol., A **63**, 367 (1992).
[51] J. H. Braun, A. Baidins, and R. E. Marganski, Prog. Org. Coat. **20**, 105 (1992).
[52] H. D. Akhtar, S. E. Pratsinis, and S. V. R. Mastrangelo, J. Mater. Res. **9**, 1241 (1994).
[53] S. Paul, *Surface Coatings, Science and Technology*, 2nd ed. (Wiley, Chichester, 1996).
[54] M. L. Taylor, G. E. Morris, and R. S. C. Smart, J. Colloid Interface Sci. **262**, 81 (2003).
[55] J. P. Perdew and Y. Wang, Phys. Rev. B **45**, 13244 (1992).
[56] J. P. Perdew, J. A. Chevary, S. H. Vosko, K. A. Jackson, M. R. Pederson, D. J. Singh, and C. Fiolhais, Phys. Rev. B **46**, 6671 (1992).
[57] T. Bredow and A. R. Gerson, Phys. Rev. B **61**, 5194 (2000).
[58] M. M. Islam, V. V. Maslyuk, T. Bredow, and C. Minot, J. Phys. Chem. B **109**, 13597 (2005).
[59] M. M. Islam, T. Bredow, and C. Minot, Chem. Phys. Lett. **418**, 561 (2006).
[60] M. M. Islam, T. Bredow, and C. Minot, J. Phys. Chem. B **110**, 9413 (2006).
[61] M. M. Islam, T. Bredow, and C. Minot, J. Phys. Chem. B **110**, 17518 (2006).
[62] V. V. Maslyuk, M. M. Islam, and T. Bredow, Phys. Rev. B **72**, 125101 (2005).
[63] V. R. Saunders, R. Dovesi, C. Roetti, R. Orlando, C. M. Zicovich-Wilson, N. M. Harrison, K. Doll, B. Civalleri, I. Bush, Ph. D'Arco, and M. Llunell, *CRYSTAL2003 User's Manual* (University of Torino, Torino, 2003).
[64] T. Bredow, L. Giordano, F. Cinquini, and G. Pacchioni, Phys. Rev. B **70**, 035419 (2004).
[65] B. Montanari, B. Civalleri, C. M. Zicovich-Wilson, and R. Dovesi, Int. J. Quantum Chem. **106**, 1703 (2006).
[66] E. Apra', M. Causá, M. Prencipe, R. Dovesi, and V. R. Saunders, J. Phys.: Condens. Matter **5**, 2969 (1993).
[67] C. Pisani, R. Dovesi, and C. Roetti, *Hartree-Fock Ab Initio Treatment of Crystalline Systems*, Lecture Notes in Chemistry Vol. 48 (Springer-Verlag, Heidelberg, 1988).
[68] H. J. Monkhorst and J. D. Pack, Phys. Rev. **13**, 5188 (1976).
[69] K. Rościszewski, K. Doll, B. Paulus, P. Fulde, and H. Stoll, Phys. Rev. B **57**, 14667 (1998).
[70] *CRC Handbook of Chemistry and Physics*, 77th ed. (CRC, Boca Raton, FL, 1997).
[71] M. Lazzeri, A. Vittadini, and A. Selloni, Phys. Rev. B **63**, 155409 (2001).
[72] J. Muscat, V. Swamy, and N. M. Harrison, Phys. Rev. B **65**, 224112 (2002).
[73] R. Dovesi, V. R. Saunders, C. Roetti, R. Orlando, C. M. Zicovich-Wilson, F. Pascale, B. Civalleri, K. Doll, N. M. Harrison, I. J. Bush, Ph. D'Arco, and M. Llunell, *CRYSTAL06 User's Manual* (University of Torino, Torino, 2006).
[74] M. H. Manghnani, S. Fisher, Jr., and W. S. Brower, J. Phys. Chem. Solids **33**, 2149 (1972).
[75] L. Gerward and J. S. Olsen, J. Appl. Crystallogr. **30**, 259 (1997).
[76] O. V. Kovalev, *Representations of the Crystallographic Space Groups: Irreducible Representations, Induced Representations, and Corepresentations* (Gordon and Breach, Philadelphia, 1993).
[77] P. A. Cox, *The Electronic Structure and Chemistry of Solids* (Oxford University Press, Oxford, 1987), Chap. 3.
[78] J. Sasaki, N. L. Peterson, and K. Hoshino, J. Phys. Chem. Solids **46**, 1267 (1985).
[79] A. Boronicolos and J. C. Vickerman, J. Catal. **100**, 59 (1986).
[80] J. F. Stebbins, I. Farnan, and U. Klabunde, J. Am. Ceram. Soc. **72**, 2198 (1989).
[81] K. S. Forland, Acta Chem. Scand. (1947-1973) **20**, 2573 (1966).
[82] R. A. Slepetys and P. A. Vaughan, J. Phys. Chem. **73**, 2157 (1969).
[83] U. Gesenhues and T. Rentschler, J. Solid State Chem. **143**, 210 (1999).
[84] M. F. Yan and W. W. Rhodes, J. Appl. Phys. **53**, 8809 (1982).
[85] J. A. Ikeda, Y-M. Chiang, and B. D. Fabes, J. Am. Ceram. Soc. **73**, 1633 (1990).
[86] D. C. Sayle, C. R. A. Catlow, M. A. Perrin, and P. Nortier, J. Phys. Chem. Solids **56**, 799 (1995).
[87] M. Steveson, T. Bredow, and A. Gerson, Phys. Chem. Chem. Phys. **4**, 358 (2002).
[88] J. Nowotny, M. Radecka, and M. Rekas, J. Phys. Chem. Solids **58**, 927 (1997).
[89] J. Yahia, Phys. Rev. **130**, 1711 (1963).